Silicon Based Ultra Wide Discrete Band Conversion

Ozdal Boyraz[a,b] ,En-Kuang Tien[a] and Shiming Gao[a,c]

[a]Department of Electrical Engineering & Computer Sci., University of California, Irvine, CA, 92697
[b]College of Engineering and Natural Sciences, Istanbul Sehir University, Istanbul, Turkey, 34396
[c] Centre for Optical and Electromagnetic Research, Zhejiang University, Hanghou 310058, China

ABSTRACT

Nonlinear silicon photonics has been an immense research subject in the past several years with promising prospects of delivering chip scale signal modulation, shaping and characterization tools. In particular, broadband parametric process has been considered for applications ranging from wideband light amplifiers to signal characterization and signal shaping tools. Although underlying nonlinear effect, Kerr phenomena, in silicon has generated promising result of wavelength conversion, the success of these devices have been challenged by the presence of nonlinear losses such as two photon absorption and the two photon generated free carrier absorption. Experimental demonstrations were limited to conversion efficiencies below -10dB. Here, we present the prospect of ultra wide discrete band conversion schemes and the prospect of parametric process at mid-infrared wavelengths where nonlinear losses are not present. In particular, we explore the parametric wavelength conversion scheme at mid-wave infrared wavelength (2μm~6μm) by four-wave-fixing process in silicon waveguides with new cladding materials, such as sapphire, that can provide transparency up to 6μm and facilitate phase matching condition for discrete wavelength bands as far as 60THz away from each other. Design criteria include the optimization of mode overlap integrals and dispersion engineering for an ultra-wide band signals. The particular results of wavelength conversion between 2μm bands and 5μm bands, and between 1.8μm bands and >4μm bands will be presented. Prospects of frequency band conversion in generation of new infrared signals and low noise, room temperature detection of mid-infrared signals will also be discussed.

Keywords: Silicon waveguide, mid-wave infrared, nonlinear optics, four wave mixing.

I. INTRODUCTION

Silicon photonics has the potential of delivering chip scale linear and nonlinear optical devices suitable for optical communication systems. In particular, the large index contrast and relatively large nonlinear coefficient of silicon offers an attractive platform for silicon nonlinear photonic devices with electrooptic tunability and high density planar photonic devices that can be integrated with CMOS IC. Up to date, Raman amplifier [1, 2], Raman laser [3-5] and parametric amplification and conversion [6-11] have been demonstrated in silicon waveguides to assist optical signal processing at telecomm applications. However, the high efficiency operation of these devices are challenged by nonlinear impediments such as two photon absorption and free carrier absorption [12]. Mid wave infrared (MWIR), defined as the wavelength range from 2μm to 6μm, has potential for silicon photonics because 1) crystalline silicon has a good transparency windows for wavelengths from near infrared wavelength of 1.2μm all the way to MWIR wavelength of 6.6μm 2) Nonlinear losses such as two photon absorption can be negligible in the MWIR range [13].

MWIR has attracted a lot of attention for gas sensing application and thermal imaging for civil and military application due to the 2μm-5μm air transmission window. MWIR spectral window also has potential applications such as optical sensing, free space communication, thermal and biomedical imaging. Up to date, quantum cascade laser and quantum well based on III-V materials are being offered as major light sources and receivers at these wavelengths

(>3μm) [14, 15]. Additionally, fiber lasers from 2μm to 3μm are available based on fluoride fiber doped with holmium (2.1μm and 2.9μm) [16, 17], thulium (1.8-2.3μm) [18] and erbium (2.7μm) [19]. However, little effort has been made on silicon photonics in MWIR wavelengths [13]. Recently, the demonstration of cascaded Raman laser has proven the possibility of generating long wavelength lasers starting with a 1550nm pump [20]. Also, the measurement of 12dB of Raman gain at 3.4 μm illustrates the strength of silicon as a rare light amplifier at those wavelengths [21]. Moreover, research on design and fabrication of waveguides suitable for MWIR wavelengths has been demonstrated. Although silicon is transparent at MWIR wavelengths, silicon waveguides are usually fabricated on silicon on insular (SOI) wafers where the insulator can be opaque at these wavelengths. For instance, the silicon dioxide, which is the most commonly used insular in SOI wafers, has attenuation coefficient as high as 10dB/cm in MWIR wavelengths except for the 2.9μm-3.5μm window, as shown in Fig. 1, [22]. Hence, alternative insular materials or different waveguide structure must be adapted for MWIR applications. Several possible solutions have been proposed such as free standing waveguide with air cladding and hollow core waveguides with Bragg reflector surroundings [23]. Alternatively, by Soref *et al* have proposed using silicon on different substrates such as silicon nitride or Sapphire [24]. Sapphire (Al_2O_3) is <80% transparent from visible to 5.5μm [22] and SOS wafer is commercially available.

In this paper, we present the dispersive and nonlinear properties of silicon waveguides suitable for MWIR applications by applying mode analysis and analytical modeling of silicon rib waveguides with sapphire substrate and air claddings. We show that dispersion engineering in these waveguides facilitate modulational instability based frequency band conversion that that can create phase and amplitude replica of MWIR signals at wavelengths as low as 1.5um. Here, we show that rib waveguides with air cladding can provide -10dB conversion efficiencies between 2.8μm and 6.2μm and also 1.5μm and 4.5μm at pump intensities up to 1 GW/cm^2. Frequency band conversion relies on waveguides with nonzero local dispersion values and provides phase matching for discrete wavelength bands. Further optimization of the waveguide geometry may also facilitate ultra broadband frequency conversion in silicon waveguides.
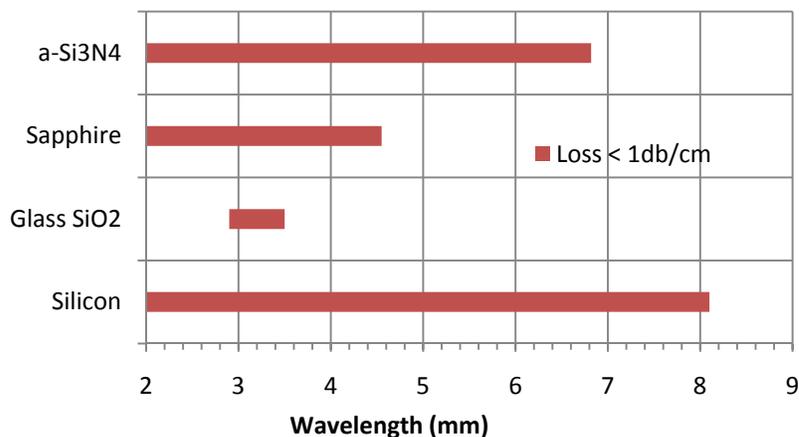
Figure 1. 1dB/cm transmission spectrum of the materials for MWIR silicon devides.

II. DISPERSION AND NONLINEARITY AT MWIR

2.1. Kerr nonlinearity in MWIR

Kerr effect is a third order nonlinear effect which induce intensity dependent refractive index change. The index change contributes to various nonlinear effects, such as self phase modulation, cross phase modulation and four wave mixing. In MWIR wavelengths (2μm to 6μm), it is well known that n_2 will scale down with the increasing wavelength of

operation. Detailed theoretical models have been presented to describe the dispersion of third order nonlinearity include TPA and Kerr nonlinearity in silicon [25-27]. Therefore, the nonlinear index change n_2 can be calculated from two photon absorption coefficient using Kramer-Kronig relation. Here, nonlinear index n_2 = 4.5e-14 cm/Gw at 1550nm is used for fit the theoretical curve to find the approximate n_2 at MWIR wavelength. Here we illustrate the scaling of n_2 with respect to the photon energy that is normalized by the bandgap energy of silicon (i.e $h\nu/E_g$ where E_g is the bandgap energy of silicon) in Figure 2. Results indicate that n_2 scales down by factor of 2 from 2μm to 6μm.
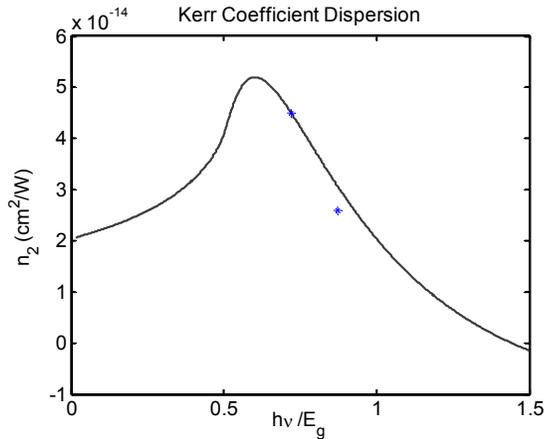
Figure 2. Predicted n_2 dispersion as function of relative photon energy.

2.2. Material and Waveguide Dispersion

It is a known fact that silicon has normal dispersion at wavelengths up >8μm. On the other hand cladding materials commonly used in silicon photonic devices have anomalous dispersion at these wavelengths that facilitate the dispersion engineering at planar silicon devices. For instance, Figure 3 illustrates the material dispersion of silicon and two common cladding materials: sapphire and SiO_2. Since sapphire has a material dispersion that has the opposite sign of the material dispersion of silicon in MWIR region, the selection of sapphire in selected waveguide geometries provides waveguide dispersion that can compensate the material dispersion. As a result, sapphire on silicon bodes well with low loss and low dispersion requirements for parametric devices envisioned at longer wavelengths.
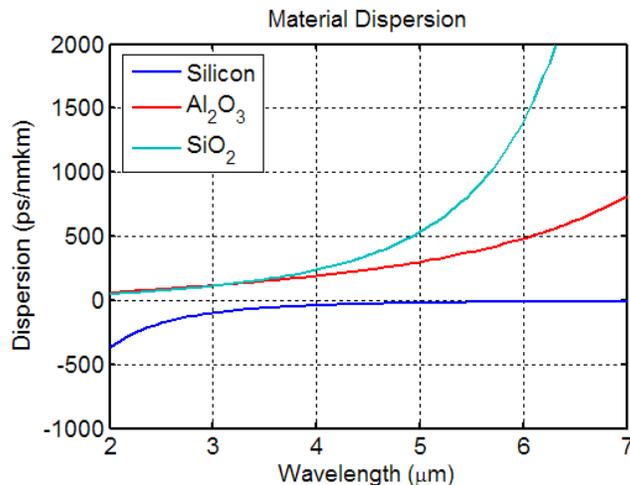
Figure 3. Material dispersion of silicon, sapphire ,SiO2 and silicon nitride.

In this manuscript we investigate the nonlinear and dispersive properties of rib waveguides and channel waveguides,

as shown in Figure 4(a), for MWIR parametric amplifier. Here, silicon on sapphire waveguide is used to enable low loss in mid-IR region. First, we investigate the single mode condition, mode confinement, the effective waveguide index, and modal area (A_{eff}) by calculating the optical mode profile in the waveguide by using FEM method (Comsol). Then, the dispersion D (or β_2) are obtained from the effective index profile at various wavelengths by using:

$$D = -\frac{2\pi c}{\lambda^2}\beta_2 = \frac{\lambda}{c}\frac{d^2 n}{d\lambda^2} \tag{1}$$
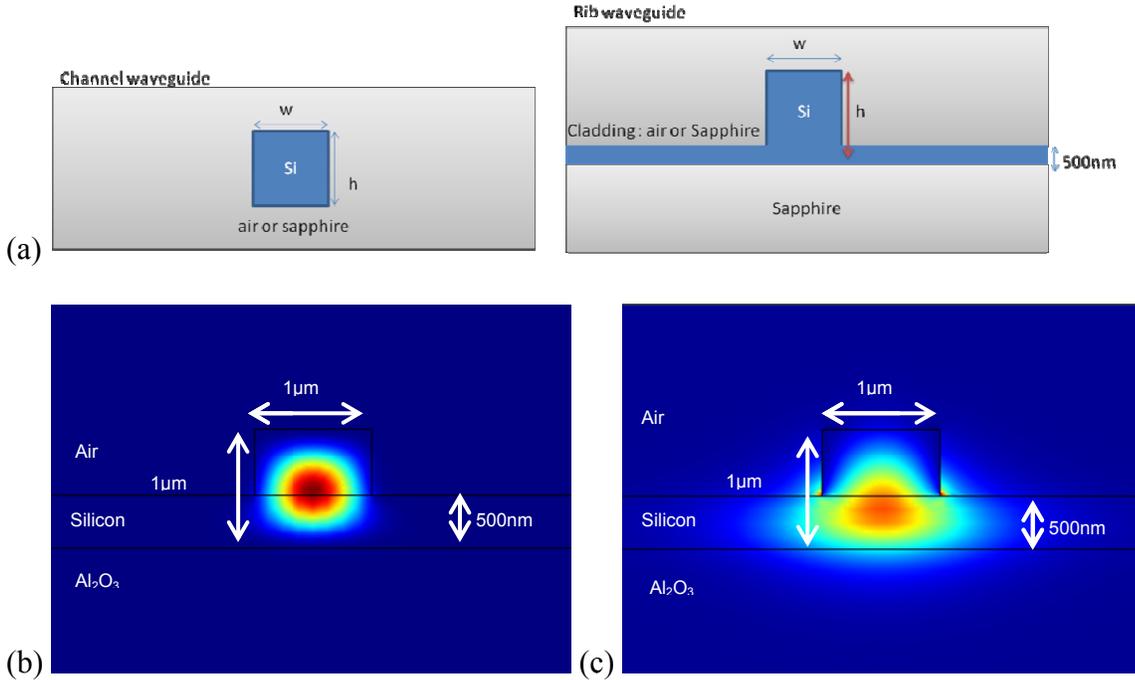
Figure 4. (a) The proposed waveguide structure and the mode profiles of the rib waveguide at (b) 2μm and (c) 5μm.

For instance, Figure 4(b) and Figure 4(c) illustrate the mode profile in a 1μm x 1μm rib waveguide with 500nm slab solved by FEM method at wavelengths of 2μm and 5μm, respectively.
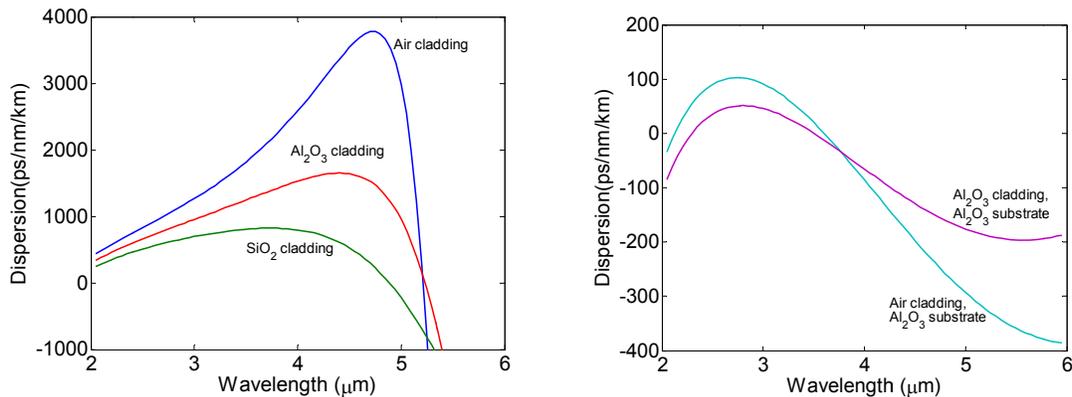
Figure 5. (a) The calculated dispersion of channel waveguide with air, sapphire and SiO₂ as cladding materials. (b) Dispersion for rib/ridge waveguide with sapphire substrate and air and sapphire cladding.

The dispersion of channel and rib waveguides with air and sapphire cladding with height and width of 1µm by 1µm is shown in Figure 5. The dispersion of the waveguide is estimated to be D<*200ps/km/nm* for wavelengths range from 2µm to 6µm in a 1µm by 1µm waveguide with both air and sapphire cladding, Fig. 5 (a). These low dispersion values are particularly important and suitable for broadband continuous wavelength conversion in the presence of high nonlinearity.

(a)
(b)
(c)
(d)
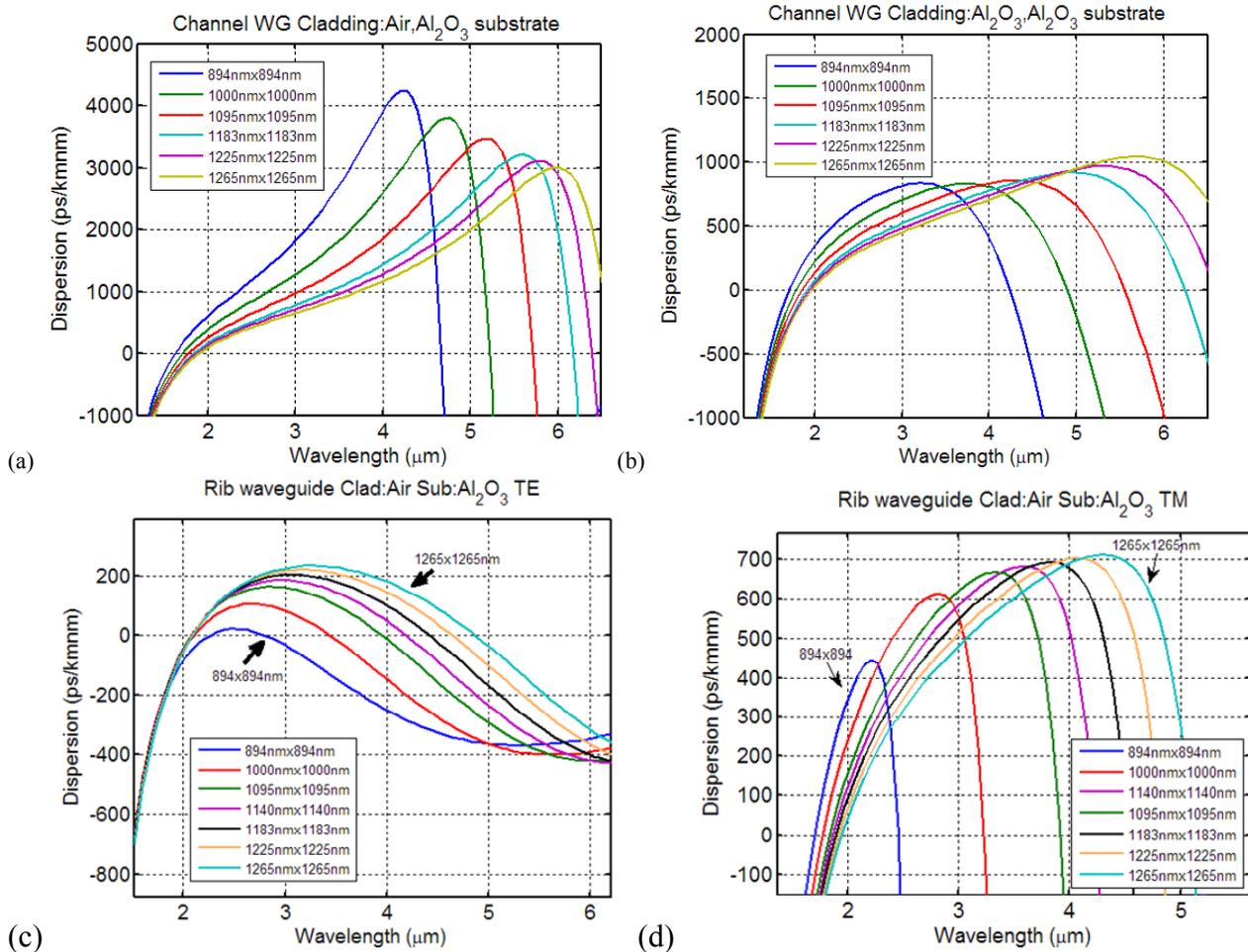
Figure 6. Dispersions of the channel waveguide surrounded by (a)air and (b) Sapphire and rib waveguide on sapphire with air cladding for (c)TE and (d)TM mode.

Figure 6 illustrates the detailed analysis of total dispersion in silicon waveguides with different geometries. Here the study of dispersion scaling is performed by calculating the dispersion with respect to the cross sectional areas of the waveguides (width×height) from $0.8µm^2$ to $1.6µm^2$. Figure 6(a) shows dispersion of TE wave of symmetric channel waveguides surrounded by air (free standing waveguide) and Fig. 6(b) shows the dispersion of channel waveguides surrounded by sapphire. The first advantage of sapphire cladding waveguides comes from its ability to produce lower dispersion values in the same geometry, which is maintained in less than 1000ps/nm/km as illustrated in Fig 6(b). Also, the zero dispersion wavelength (ZDWLs) in channel waveguides surrounded by air (free standing waveguide) can be tuned from 1.6µm to 1.8µm by changing the cross sectional area, as illustrated in Fig. 6(a). Further dispersion engineering can be achieved by switching from channel waveguide to a rib waveguide and by adding 500nm of slab region. For instance, ZDWLs of the TE mode can be controlled from 2.8µm- 4.9µm in the rib waveguide on air cladding, Fig. 6(c)(d) by increasing the cross sectional area from $0.8µm^2$ to $1.6µm^2$ with the same slab region. Also, the dispersion

in these waveguides can be maintained within 200ps/nm/km at wavelengths from 2μm to 5μm. The results indicate that, with similar waveguide geometry, waveguide dispersion, and hence the total dispersion of the silicon waveguide, can be drastically changed to provide a means to control the zero-dispersion-wavelength.

III.   III. DISPERSION ENGINEERING IN MWIR REGION FOR PARAMETRIC PROCESS

Low dispersion waveguides are particularly important for broadband parametric wavelength conversion and amplification that require phase matching between the pump, signal and idler waves. The theory behind FWM process is well investigated and it can be described as the coupling equations [8, 28, 29]:

$$\frac{\partial A_p}{\partial z} = i\left(\gamma_p \left|A_p\right|^2 + 2\gamma_{pi}\left|A_i\right|^2 + 2\gamma_{ps}\left|A_s\right|^2\right)A_p + 2\gamma_{FWM} A_i A_s A_p^* e^{i\Delta k_{Linear}z} \tag{2}$$

$$\frac{\partial A_i}{\partial z} = i\left(\gamma_i \left|A_i\right|^2 + 2\gamma_{is}\left|A_s\right|^2 + 2\gamma_{ip}\left|A_p\right|^2\right)A_i + \gamma_{FWM} A_p^2 A_i^* e^{i\Delta k_{Linear}z} \tag{3}$$

$$\frac{\partial A_s}{\partial z} = i\left(\gamma_s \left|A_s\right|^2 + 2\gamma_{si}\left|A_i\right|^2 + 2\gamma_{sp}\left|A_p\right|^2\right)A_i + \gamma_{FWM} A_p^2 A_s^* e^{i\Delta k_{Linear}z} \tag{4}$$

Here the linear loss and free carrier effect are ignored. A_p, A_s and A_i are the electric field amplitude of pump, signal and idler, respectively. The first term represents the nonlinear term involves self phase modulation (γ_x, x=p, s, i) and cross phase modulation (γ_{xy} x,y=p, s, i) of pump, signal and idler. The second term in the equations represents four wave mixing where γ_{FWM} is the nonlinear coefficient involved with pump, signal and idler. γ is proportional to Kerr index n_2 and it is calculated by $\gamma = 2\pi n_2/\lambda A_{eff}$. Here, the nonlinear coefficient is determined by using the dispersion relationship mentioned in the previous section. To obtain γ_{xy}, we use the Kerr coefficient at the averaged frequency, $\tilde{\omega}_{xy} = \left(\omega_x + \omega_y\right)/2$. For γ_{FWM}, Kerr coefficient at pump frequency is used. The effective area A_{eff} is calculated from the overlap integral of all the involved modes. The difference in propagation constant (Δk_{Linear}) between pump, signal and idler waves is calculated as: $\Delta k_{linear} = k_{signal} + k_{idler} - 2k_{pump}$, where k_{pump}, k_{signal}, k_{idler} represent the propagation constants of pump, signal and idler waves, respectively. The equations are usually solved using numerical method but a simple analytical expression can be obtained by assuming non depleted pump. The parametric gain can be written as [30]:

$$G = \frac{P_s(L)}{P_s(0)} = 1 + \left[\frac{\gamma_{FWM} P_{pump}}{g}\sinh(gL)\right]^2 \tag{5}$$

Where $g = \left[\left(\gamma_{FWM} P_{pump}\right)^2 - \left(\Delta k/2\right)^2\right]^{\frac{1}{2}}$ is the parametric gain parameter, and L is the interaction length. The parametric conversion efficiency G_c can be written as $G_c = G-1$. In order to achieve phase matching, the aggregate phase shifts due to linear and nonlinear effects should be minimized. It is written as:

$$\Delta k = \Delta k_{linear} + \Delta k_{nonlinear} \tag{6}$$

Here $\Delta k_{nonlinear} = 2\left(\gamma_{ip} + \gamma_{sp} - \gamma_p\right)P_{pump}$ represents the nonlinear phase mismatch induced by the Kerr nonlinearity. And also from the conservation of energy $2\omega_{pump} = \omega_{signal} + \omega_{idler}$ is required.

Under small gain, the bandwidth of the parametric amplifier is proportional to the square root of the product the $\beta_2 L$, which implies that the bandwidth of the parametric process can be improved by decreasing the dispersion of the waveguide. To achieve net gain, the phase mismatch term Δk should be reduced to near zero values. Conventionally, The phase match is achieved by pumping at near ZDWL to cancel the wavenumber mismatch between the signal and the

idler. Since the dispersion is nearly linear around ZDWL, the phase matching is satisfied, as illustrated in Figure 7 (a). In this paper, since SOS waveguide exhibit the two zero dispersion wavelengths, the pump can be selected away from the ZDWL. The phase matching condition is satisfied not only near the pump wavelength, but also the other discrete band which is 2 μm away from the pump wavelength, Fig. 7(b). The dispersion of the pump and signal in Figure 7(b) shows that the positive dispersion of pump and anti-stoke signal can be compensate by the larger negative dispersion values of the stoke signal and the total phase mismatch is zero at the two signal wavelengths. With the phase matching condition satisfied, we expect that modulation instability is achieved within a narrow band far away from the pump wavelength. Figure 7(b) shows that the wavelength can be convert from 6.2 μm to 2.6μm. This behavior have been shown with similar dispersion profiles in photonic crystal fibers [31] and has been proposed in silicon waveguides at communication wavelengths [8, 9] with mode profiles not suitable for long wavelength operations.
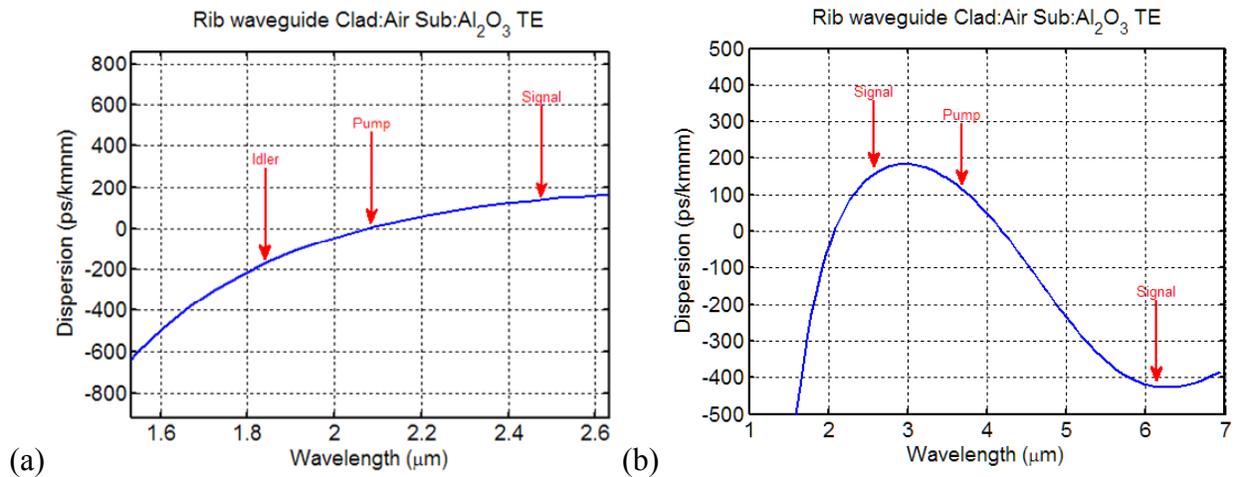
Figure 7. Phase matching concept of (a) conventional phasematching and (b) discrete band phase matching.

IV. IV. FOUR WAVE MIXING SIMULATION RESULTS

Discrete and continuous wavelength conversion is demonstrated in dispersion optimized silicon waveguides. We use 1.3μm^2 (1.14×1.14μm) single mode silicon waveguides supporting long wavelength operations and built on SOS with air cladding. Unlike conventional wavelength conversion, the nonlinear dispersion profile is being utilized by using a pump laser 700nm away from the zero dispersion wavelengths, Fig. 7(b). The phase matching condition is satisfied at pump wavelength and a discrete band, where large negative dispersion at long wavelength compensates the low positive dispersion at pump wavelength. Fig. 8(a) shows the phase mismatch $\Delta\beta$ for a 1.3μm^2 (1140nm×1140nm) waveguide at a pump wavelength away from the zero dispersion wavelengths. Under discrete wavelength conversion the silicon operates in parametric regime at the vicinity of the pump laser and achieves the modulation instability at a discrete wavelength band 1.5μm when the gain coefficient g is real number, Fig. 8(b). The corresponding conversion efficiency at those wavelengths is shown in Fig. 8(c). -8dB conversion efficiency is achieved where the phase matching condition is satisfied with 1GW/cm^2 pump power. For example, we show that for pumping at 3.76μm, wavelength conversion between 2.8um and 6.2um is possible with conversion band of 15 nm, Fig. 8(d). We also show that using different waveguide geometries provide wavelength conversion between bands from 2um to 6um and opens a possibility that long range wavelength conversion that convert MWIR to communication wavelength. In addition, pump wavelength is critical to the phase matching wavelengths. Figure 9 shows the phase matching wavelengths with respect of pump wavelength in the 1.3 μm^2 rib waveguide. It is clear that with this approach the phase matching to convert wavelengths separated by more than 3.5μm is feasible.

(a) (b)

(c) (d)
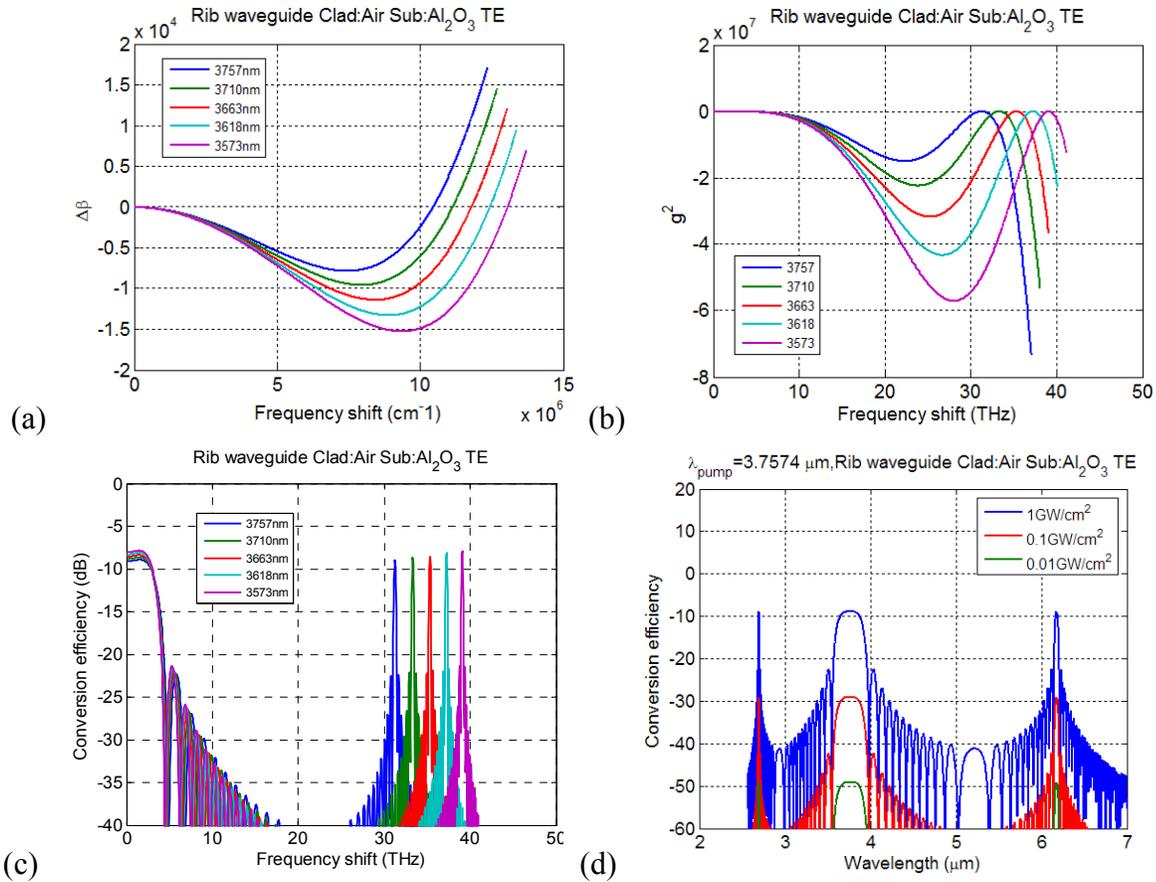
Figure 8. (a) For 1.3μm² waveguide at TE polarization, phase matching condition $k_{signal}+\Delta k_{idler}-\Delta k_{pump}=0$ is satisfied for signal away from the pump wavelength. (b) Parametric gain g^2 for the 1.14μm×1.14μm waveguide at different wavelengths. Notice the gain happens when $g^2 > 0$. (c) Conversion efficiency at several pump wavelengths. (d) The conversion efficiency for 3.757μm pump wavelength which shows a discrete parametric conversion from 6.2μm to 2.8μm.
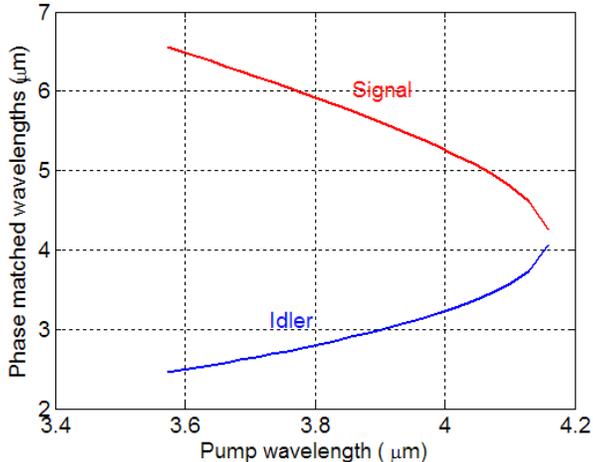
Figure 9. Phase matching wavelengths ($\Delta k=0$) for rib waveguide with 500nm slab region. Pump power is set at 0.1GW/cm².

In addition to conversion with in mid-IR, wavelength conversion between MWIR and telecommunication wavelength has great potential for MWIR detection and free space communication applications. By scaling the waveguide dimension,

we find that phase matching condition can be satisfied between 1.5μm and ~5μm in a 1μm by 1μm waveguide with 500nm slab height. The dispersion of the TE mode in such waveguide is shown in Fig. 6(d). The zero dispersion wavelengths are at 2.1μm and 3.5μm. The phase matching condition can be satisfied at 1.55 μm and 5.1μm and the conversion efficiencies of varies pump intensities are illustrated in Fig 10. While pump at 2.4μm, -20dB conversion efficiency is achievable with 0.1 GW/cm^2 and The efficiencies can increase up to -3dB with 1GW/cm^2 pump power, Fig 10. Note that the pump wavelength is beyond half of silicon band gap and it does not suffer from TPA. The conversion bandwidth is 2nm at 1.55μm and 20nm at 5.1μm.The phase matching condition with respect of pump wavelength is shown in Fig. 11.
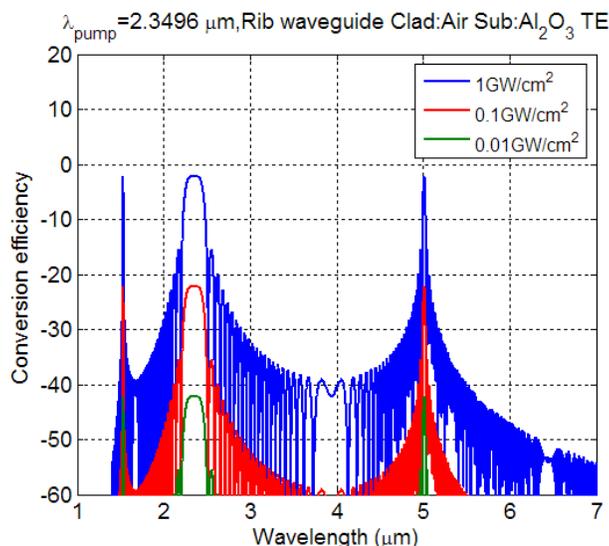
Figure 10. Conversion efficiency for 1GW/cm^2, 0.1GW/cm^2 and 0.01GW/cm^2 pump intensity at 2.4μm. the maximum conversion efficiency is 0dB, -20dB and -40dB, respectively.
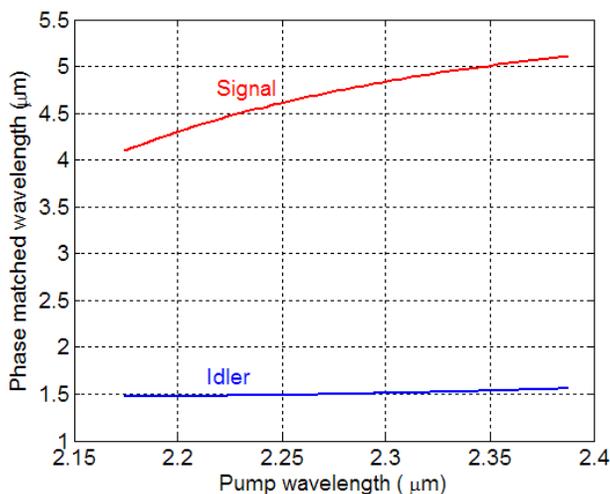
Figure 11. Phase matching condition for 1μm by 1μm rib waveguide with 500nm slab region. Pump power is set at 0.1GW/cm^2.

V. CONCLUSION

MWIR in silicon has great potential for next generation optical communication applications. We show that by

manipulating the waveguide dimensions, the zero dispersion wavelengths can be tuned from 4 μm to 5 μm. We estimate that >3μm discrete wide-band conversion in mid-IR achievable at 3.7μm pumping with ~-10dB conversion efficiency in a 1cm long waveguide with intensity at 1GW/cm^2. We also show that 2μm pump wavelengths shows possible conversion from 4-5μm to telecommunication wavelengths at 1.5μm.

Reference

[1]   O. Boyraz and B. Jalali, "Demonstration of 11dB fiber-to-fiber gain in a silicon Raman amplifier," *IEICE Electronics Express,* vol. 1, pp. 429-434, 2004.

[2]   R. Claps, D. Dimitropoulos, V. Raghunathan, Y. Han, and B. Jalali, "Observation of stimulated Raman amplification in silicon waveguides," *Optics Express,* vol. 11, pp. 1731-1739, Jul 2003.

[3]   O. Boyraz and B. Jalali, "Demonstration of a silicon Raman laser," *Optics Express,* vol. 12, pp. 5269-5273, Oct 2004.

[4]   H. S. Rong, A. S. Liu, R. Jones, O. Cohen, D. Hak, R. Nicolaescu, A. Fang, and M. Paniccia, "An all-silicon Raman laser," *Nature,* vol. 433, pp. 292-294, Jan 2005.

[5]   X. Z. Sang, E. K. Tien, N. S. Yuksek, F. Qian, Q. Song, and O. Boyraz, "Dual-wavelength mode-locked fiber laser with an intracavity silicon waveguide," *Ieee Photonics Technology Letters,* vol. 20, pp. 1184-1186, Jul-Aug 2008.

[6]   M. A. Foster, A. C. Turner, J. E. Sharping, B. S. Schmidt, M. Lipson, and A. L. Gaeta, "Broad-band optical parametric gain on a silicon photonic chip," *Nature,* vol. 441, pp. 960-963, Jun 2006.

[7]   M. A. Foster, A. C. Turner, R. Salem, M. Lipson, and A. L. Gaeta, "Broad-band continuous-wave parametric wavelength conversion insilicon nanowaveguides," *Optics Express,* vol. 15, pp. 12949-12958, 2007.

[8]   Q. Lin, T. J. Johnson, R. Perahia, C. P. Michael, and O. J. Painter, "A proposal for highly tunable optical parametric oscillation in siliconmicro-resonators," *Optics Express,* vol. 16, pp. 10596-10610, 2008.

[9]   Osgood, Jr., N. C. Panoiu, J. I. Dadap, X. Liu, X. Chen, I. W. Hsieh, E. Dulkeith, W. M. Green, and Y. A. Vlasov, "Engineering nonlinearities in nanoscale optical systems: physics and applications in dispersion-engineered silicon nanophotonic wires," *Advances in Optics and Photonics,* vol. 1, pp. 162-235, 2009.

[10]   X. Zhang, S. Gao, and S. He, "Optimal Design of a Silicon-on-Insulator Nanowire Waveguide for Broadband Wavelength Conversion," *Progress in Electromagnetics Research-Pier,* vol. 89, pp. 183-198, 2009.

[11]   S. Gao, X. Zhang, Z. Li, and S. He, "Polarization-Independent Wavelength Conversion Using an Angled-Polarization Pump in a Silicon Nanowire Waveguide," *Selected Topics in Quantum Electronics, IEEE Journal of,* vol. 16, pp. 250-256.

[12]   X. Sang and O. Boyraz, "Gain and noise characteristics of high-bit-ratesilicon parametric amplifiers," *Optics Express,* vol. 16, pp. 13122-13132, 2008.

[13]   B. Jalali, V. Raghtmathan, R. Shori, S. Fathpour, D. Dimitropoulos, and O. Stafsudd, "Prospects for silicon mid-IR Raman lasers," *Ieee Journal of Selected Topics in Quantum Electronics,* vol. 12, pp. 1618-1627, Nov-Dec 2006.

[14]   P. Werle, F. Slemr, K. Maurer, R. Kormann, R. Mucke, and B. Janker, "Near- and mid-infrared laser-optical sensors for gas analysis," *Optics and Lasers in Engineering,* vol. 37, pp. 101-114, Feb-Mar 2002.

[15]   F. Capasso, R. Paiella, R. Martini, R. Colombelli, C. Gmachl, T. L. Myers, M. S. Taubman, R. M. Williams, C. G. Bethea, K. Unterrainer, H. Y. Hwang, D. L. Sivco, A. Y. Cho, A. M. Sergent, H. C. Liu, and E. A. Whittaker, "Quantum cascade lasers: Ultrahigh-Speed operation, optical wireless communication, narrow linewidth, and far-infrared emission," *Ieee Journal of Quantum Electronics,* vol. 38, pp. 511-532, Jun 2002.

[16]   S. D. Jackson and T. A. King, "High-power diode-cladding-pumped Tm-doped silica fiber laser," *Optics Letters,* vol. 23, pp. 1462-1464, Sep 15 1998.

[17]   S. D. Jackson, "Single-transverse-mode 2.5-W holmium-doped fluoride fiber laser operating at 2.86 mu m," *Optics Letters,* vol. 29, pp. 334-336, Feb 15 2004.

[18]   R. Allen and L. Esterowitz, "Cw Diode Pumped 2.3-Mu-M Fiber Laser," *Applied Physics Letters,* vol. 55, pp. 721-722, Aug 21 1989.

[19]   S. Tokita, M. Murakami, S. Shimizu, M. Hashida, and S. Sakabe, "Liquid-cooled 24 W mid-infrared Er:ZBLAN fiber laser," *Optics Letters,* vol. 34, pp. 3062-3064, Oct 15 2009.

[20]   H. S. Rong, S. B. Xu, O. Cohen, O. Raday, M. Lee, V. Sih, and M. Paniccia, "A cascaded silicon Raman laser," *Nature Photonics,* vol. 2, pp. 170-174, Mar 2008.

[21]   V. Raghunathan, D. Borlaug, R. R. Rice, and B. Jalali, "Demonstration of a mid-infrared silicon Raman

amplifier," *Optics Express,* vol. 15, pp. 14355-14362, Oct 2007.

[22]   P. Klocek, *Handbook of Infrared Optical Materials*. New York: M. Dekker, 1991.

[23]   P. Yang, S. Stankovic, J. Crnjanski, E. Teo, D. Thomson, A. Bettiol, M. Breese, W. Headley, C. Giusca, G. Reed, and G. Mashanovich, "Silicon photonic waveguides for mid- and long-wave infrared region," *Journal of Materials Science: Materials in Electronics,* vol. 20, pp. 159-163, 2009.

[24]   R. A. Soref, S. J. Emelett, and A. R. Buchwald, "Silicon waveguided components for the long-wave infrared region," *Journal of Optics a-Pure and Applied Optics,* vol. 8, pp. 840-848, Oct 2006.

[25]   M. Dinu, "Dispersion of phonon-assisted nonresonant third-order nonlinearities," *Quantum Electronics, IEEE Journal of,* vol. 39, pp. 1498-1503, 2003.

[26]   M. Dinu, F. Quochi, and H. Garcia, "Third-order nonlinearities in silicon at telecom wavelengths," *Applied Physics Letters,* vol. 82, pp. 2954-2956, 2003.

[27]   H. Garcia and R. Kalyanaraman, "Phonon-assisted two-photon absorption in the presence of a dc-field: the nonlinear Franz–Keldysh effect in indirect gap semiconductors," *Journal of Physics B: Atomic, Molecular and Optical Physics,* vol. 39, pp. 2737-2746, 2006.

[28]   G. Agrawal, *Nonlinear Fiber Optics, Fourth Edition*: Academic Press, 2006.

[29]   R. Stolen and J. Bjorkholm, "Parametric amplification and frequency conversion in optical fibers," *Quantum Electronics, IEEE Journal of,* vol. 18, pp. 1062-1072, 1982.

[30]   J. Hansryd, P. A. Andrekson, M. Westlund, L. Jie, and P. O. Hedekvist, "Fiber-based optical parametric amplifiers and their applications," *Selected Topics in Quantum Electronics, IEEE Journal of,* vol. 8, pp. 506-520, 2002.

[31]   T. Andersen, K. Hilligsoe, C. Nielsen, J. Thogersen, K. Hansen, S. r. Keiding, and J. Larsen, "Continuous-wave wavelength conversion in a photonic crystal fiber with two zero-dispersion wavelengths," *Optics Express,* vol. 12, pp. 4113-4122, 2004.